

# Two-photon-assisted excited state absorption in nanocomposite films of PbS stabilized in a synthetic glue matrix

Pushpa Ann Kurian<sup>1</sup>, C Vijayan<sup>1</sup>, C S Suchand Sandeep<sup>2</sup>,  
Reji Philip<sup>2</sup> and K Sathiyamoorthy<sup>1</sup>

<sup>1</sup> Indian Institute of Technology, Madras, Chennai 600036, India

<sup>2</sup> Raman Research Institute, Bangalore 560080, India

E-mail: [cvijayan@physics.iitm.ac.in](mailto:cvijayan@physics.iitm.ac.in)

Received 15 September 2006, in final form 29 November 2006

Published 12 January 2007

Online at [stacks.iop.org/Nano/18/075708](http://stacks.iop.org/Nano/18/075708)

## Abstract

Strong nonlinear absorption is observed in nanocomposite films containing PbS nanocrystals of mean size of 3.3 nm stabilized in a commercial poly(vinyl acetate) glue by a novel and simple chemical route of synthesis. A significant blueshift of the optical absorption edge indicates strong quantum confinement. The mean nanocrystal size was characterized by x-ray diffraction and transmission electron microscopy. The surface structure of nanocrystals is analysed using infrared spectroscopy. The excitonic transitions are probed by photoacoustic spectroscopy and the results are analysed on the basis of theoretical calculations using envelope function formalism. Results of open aperture  $z$ -scan experiments suggest a model involving saturable absorption followed by two-photon absorption at a lower concentration while the data for a higher concentration fitted saturable absorption followed by three-photon absorption. Free carrier absorption due to two-photon-assisted excited state absorption appears to be the predominant mechanism of optical nonlinearity.

## 1. Introduction

Semiconductor nanocomposite films with large third-order nonlinearity and fast response continue to attract recent attention in view of their interesting physical properties as well as their potential for nonlinear optical device applications [1–3]. One of the applications is that of optical limiting based on a variety of physical mechanisms of nonlinear absorption. A large nonlinear optical response is known to be exhibited by semiconductor nanocrystals in the regime of strong quantum confinement [4, 5] where the dimension of the nanocrystal is less than the exciton Bohr diameter [6]. Bulk lead sulfide (PbS) is a direct bandgap material with a narrow bandgap of 0.41 eV and bulk exciton Bohr diameter of 18 nm. The relatively large Bohr radius makes it convenient to prepare strongly quantum confined PbS nanocrystals. However, a study of the modified physical properties of PbS nanocrystals stabilized in suitable solid host media is an area that has not received much attention in spite of its importance.

In recent years PbS nanocrystals have been fabricated in various nanoreactors like micelles [7], polymers [8–12], zeolites [13], etc. Several schemes have been used to synthesize semiconductor nanocomposites using polymer templates. Wang *et al* [14] synthesized metal sulfide nanocomposites by ion exchange of metal ions with polymer and used toxic H<sub>2</sub>S gas as the sulfide source. Semiconductor nanocomposites have been fabricated by simultaneous polymerization of monomer molecules and semiconductor nanocrystals using  $\gamma$ -irradiation. Qiao *et al* [10] have reported the synthesis of PbS/poly(vinyl acetate) nanocomposites using such a method. In this paper we present our results on the interesting optical properties of PbS nanocrystals stabilized in a commercial poly(vinyl acetate) glue which acts as a soft template to control the organization of nano building units resulting in the formation of spherical PbS nanocrystals. This method of *in situ* synthesis of homogeneously dispersed PbS nanocrystals directly in the polymer matrix at room temperature is simpler than the simultaneous polymerization of monomer molecules and

the reduction of precursors using  $\gamma$ -irradiation to prepare semiconductor nanocomposites. The main advantage of semiconductor nanocrystals dispersed in polymers is that good quality films of desired thickness can be prepared rather easily and molded into desired shapes. Further, nanocrystals dispersed in suitable solid hosts can be stabilized for long periods of time.

Interesting results have been obtained on the nonlinear optical properties of host embedded semiconductor nanocrystal systems such as CdS, CdSe, CdS<sub>1-x</sub>Se<sub>x</sub>, CdTe, etc, embedded in glass as the host matrix. However, broad size distribution [15, 16] and photodarkening are known to be limitations on using glass as the matrix. One major advantage of nanoparticles synthesized in polymers over those synthesized in glass is the low preparation temperature, not more than 200 °C [17], whereas the present work is based on a novel method of room temperature synthesis of PbS nanocrystals in synthetic glue. Earlier studies on host-embedded PbS nanocrystals (PbSNC) have focused on synthesis and characterization aspects and only a few reports are available on nonlinear optical properties [18]. Most of these are related to nonlinear refraction. Degenerate four-wave mixing technique was used to measure the third-order nonlinear optical susceptibility of PbSNC in polymer media [19]. Contributions from nonlinear refraction and nonlinear absorption cannot be extracted separately from such an experiment. The transient nonlinear optical properties of PbS nanoparticles have been studied using femtosecond time-resolved optical Kerr effect spectroscopy [20, 21]. The important part played by the surface of nanoparticles on the nonlinear refractive index has been brought out by studying the nanoparticles synthesized using different surface capping agents. Nonlinear refraction studies have been done on PbS-doped films prepared by a solgel technique in the nanosecond regime and picosecond regime using DFWM and m-line techniques [22–25]. Li *et al* [26] have done nonlinear refraction studies of PbS nanocrystals using femtosecond  $z$  scan and reported large nonlinear phase shifts though nonlinear absorption was not observed. Recently Nikesh *et al* [27] and He *et al* [28] reported the observation of two-photon absorption in the picosecond regime and three-photon absorption in the femtosecond regime, respectively, using  $z$ -scan technique for ZnS nanocrystals.

The present paper reports on the observation of large nonlinear absorption and efficient optical limiting effects in a stable nanocomposite consisting of PbS nanocrystals (NC) of mean size 3 nm dispersed in synthetic glue films prepared by a simple, room temperature method. The observed modification in nonlinear optical properties is more pronounced than that reported in other host-embedded PbS nanocrystals systems prepared by more elaborate and complicated methods. The results are discussed on the basis of underlying physical mechanisms involving free carrier absorption and multiphoton absorption.

## 2. Experimental section

Lead acetate and sodium sulfide of analytic grade are used as precursors. The host matrix used is a commercially available, transparent, water-soluble PVAc glue purchased from Crown

Chemicals Chennai, India. The composite is prepared by processing equimolar quantities of sodium sulfide and lead acetate in the glue medium, stirring continuously. The solution was poured into petri dishes and air dried to obtain stable optical quality films. The concentrations of lead acetate used are 0.5, 1, 2 and 4 mM in 50 ml aqueous solution of the glue. The four samples corresponding to these four different concentrations are designated as P0, P1, P2 and P4, respectively. The concentration of sodium sulfide used in each case is such that an equimolar ratio of Pb<sup>2+</sup>:S<sup>2-</sup> is obtained in all cases. The composite films are found to be very stable and they retain their physical properties for long periods of time. The films are of 125  $\mu$ m thickness.

Structural and size characterization is done by x-ray diffraction (XRD) on a PANalytical x-ray diffractometer. The source is a Cu K $\alpha$  line with  $\lambda = 0.15418$  nm. Tube current and voltage are 30 mA and 40 kV, respectively. The morphological characterization is done using a Jeol 3010 high resolution transmission electron microscope with an accelerating voltage of 300 kV. The IR spectrum is recorded with a Perkin Elmer Spectrum One Fourier transform infrared (FTIR) spectrophotometer which gave information about the surface of the nanocrystal. Optical absorption spectra are recorded on a Jasco V-570 spectrometer in the wavelength region 300–800 nm in which the host matrix is transparent. The photoacoustic spectroscopic studies are done by the gas microphone technique [29]. The spectrum is recorded using an automated home-built photoacoustic spectrometer. A xenon arc lamp of 500 W is used as the excitation source. The light beam selected using a monochromator (Jobin Yvon) is modulated using a mechanical chopper (SR540, Stanford Research Systems) and focused onto an airtight photoacoustic (PA) cell. The modulation frequency is 10 Hz. The PA cell consists of an aluminium cylinder with an option for inserting a microphone in its periphery. The periodically chopped beam is allowed to fall on the sample kept inside the PA cell through the transparent cell window. The nonradiative transitions within the sample heat up the boundary layer of air in contact with the sample. The periodic heating effect causes the layer to function as a vibrating piston. This results in periodic pressure fluctuations inside the cell which are detected by the sensitive microphone (G.R.A.S). The amplitude and phase angle of the PA signal are finally detected by a lock-in amplifier (SR830, Stanford Research Systems) whose reference channel is connected from the chopper. The spectral measurements are carried out at room temperature in the wavelength range of 360–720 nm in steps of 2 nm resolution. The PA spectrum is corrected for variations in source intensity as a function of wavelength using carbon black absorber for normalization. The nonlinear absorption studies are done by the  $z$ -scan technique [30] using 7 ns pulses from a Nd:YAG laser emitting at the second harmonic wavelength of 532 nm. From beam profile measurements using the knife edge method, the spatial intensity profile of the laser is found to be near-Gaussian. An automated open aperture  $z$ -scan setup is used to measure intensity-dependent transmission. The laser beam is focused using a lens of focal length 185 mm and the transmittance is measured using a pyroelectric energy probe as a function of sample position  $z$  by translating the sample along the beam axis ( $z$  axis). The sample sees a different fluence at each position

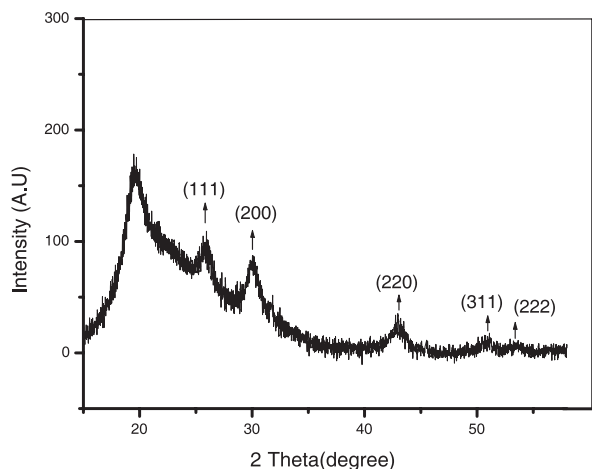


**Figure 1.** XRD pattern of PbS/glue nanocomposite P4.

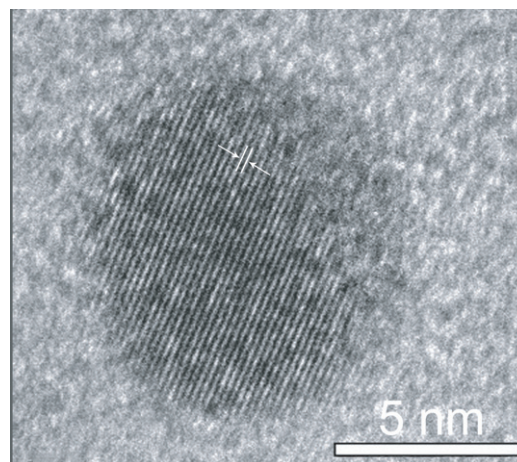


**Figure 2.** HRTEM image showing lattice planes of a single PbS nanocrystal.

of  $z$ . The small fluctuations in the pulse energy are accounted for by using a reference energy probe. The pulse to pulse energy stability is found to be approximately  $\pm 5\%$ . Depending on the absorption mechanism involved, we get a Lorentzian or inverted Lorentzian with its maximum or minimum at the focal point,  $z = 0$  where the fluence is a maximum.

### 3. Results and discussion

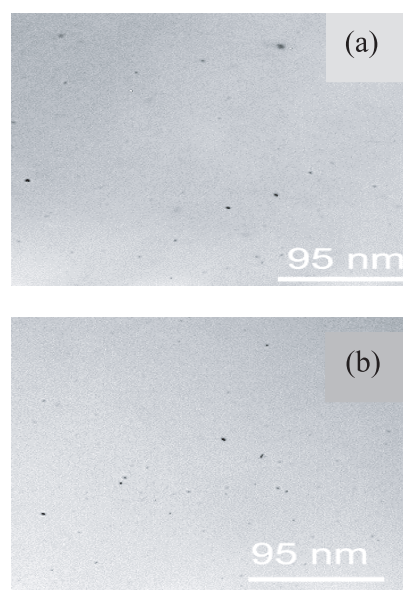
#### 3.1. Characterization by XRD, HRTEM, TEM and FTIR

Figure 1 shows the XRD pattern of sample P4. The uneven baseline is due to the presence of a larger amount of amorphous polymer component. The pattern with diffused peak structure is typical of nanocrystalline materials. The diffraction peaks observed at  $2\theta$  values of  $25.9^\circ$ ,  $30.1^\circ$ ,  $43^\circ$ ,  $51^\circ$  and  $53.5^\circ$  and the  $d$  spacing calculated indicates that the structure corresponds to the cubic rocksalt structure of PbS (JCPDS file No. 5-592). The broad peak at  $19.7^\circ$  is due to the host polymer matrix. The mean crystal size is calculated by Scherrer's formula

$$D = 0.9\lambda / \beta \cos \theta$$

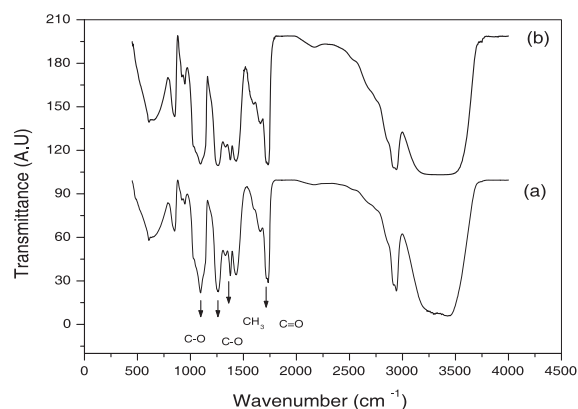
where  $D$  is the diameter of the nanocrystals,  $\lambda$  is the wavelength of the incident x-rays,  $\beta$  is the full width at half-maximum and  $\theta$  is the diffraction angle. The mean size is determined to be 4.5 nm.

Figure 2 shows the HRTEM picture of a single PbS nanocrystal embedded in the matrix. The crystallographic planes can be seen clearly in the region corresponding to the nanocrystal. The measured spacing of the planes is 0.21 nm, corresponding to the (220) plane in lattice of cubic PbS. Figures 3(a) and (b) show the TEM micrographs of samples P0 and P4, respectively. The micrographs indicate that the quasi-spherical PbS nanocrystals are homogeneously dispersed and well separated in the host matrix. The mean size and the other general features for both samples are similar in spite of the difference in concentrations. Size distribution of the nanocrystals is found to be in the range of 3–9 nm with the majority of the nanocrystals being in the 3 nm size range. The mean size of 3.3 nm is determined by evaluating 290 particles.



**Figure 3.** (a) and (b) TEM image showing PbS nanocrystals well dispersed in the host matrix for two different samples, P0 and P4, respectively.

FTIR studies are done to investigate the role of polymer molecules on the surface physics of the nanocrystal. Figure 4(a) shows the FTIR of the PVAc glue matrix. The prominent peaks observed at  $1735\text{ cm}^{-1}$  ( $\nu_{\text{C=O}}$ ),  $1095\text{ cm}^{-1}$ ,  $1263\text{ cm}^{-1}$  ( $\nu_{\text{C-O}}$ ) and  $1376\text{ cm}^{-1}$  ( $\delta_{\text{CH}_3}$ ) confirm the presence of poly(vinyl acetate). The spectrum is similar to the standard IR spectrum of poly(vinyl acetate) (Sprouse collection of IR, card no. 187-189). FTIR spectrum of the PbS-embedded glue sample P2 (figure 4(b)) is found to be identical with that of the host glue, indicating the absence of chemical bonding between the nanocrystals and host matrix. This kind of interaction between PbS nanoparticles and host matrix has been reported earlier in the case of nanoparticles in polymers such as poly(vinyl alcohol) [9] and poly(methyl methacrylate co-methacrylic acid) [11]. The mechanism of interaction between the nanocrystals and the host matrix can tentatively



**Figure 4.** FTIR spectra of (a) PVAc glue matrix, (b) PbS/glue nanocomposite P2.

be described as follows. When lead acetate is added to the aqueous solution of glue,  $\text{Pb}^{2+}$  ions are homogeneously dispersed in the matrix. The  $-\text{C}=\text{O}$  groups present in the polymer side chain interact with the  $\text{Pb}^{2+}$  ions and stabilize it. On the addition of aqueous solution of sodium sulfide, the  $\text{Pb}^{2+}$  in the host matrix reacts with  $\text{S}^{2-}$  forming PbS. PbS nanocrystals are surrounded by the polymer chains, not allowing the diffusion of PbS nanocrystals and thus controlling the growth process at room temperature.

### 3.2. Optical absorption and photoacoustic studies

Figure 5 shows the optical absorption spectrum of the PbS nanocomposite P2. The large blue shift from the bulk PbS optical absorption cutoff of 3020 nm can be clearly observed. The host matrix is transparent in the spectral range considered here. The excitonic transitions were investigated by photoacoustic spectroscopy. Figure 6 shows the photoacoustic spectrum of the nanocomposite film P2. The photoacoustic signal of host matrix is very weak and featureless in the spectral range studied here. PAS spectrum of the sample shows two peaks, one at 2.15 eV (corresponding to the peak at 578 nm) and another one at 3.04 eV (corresponding to the peak at 408 nm). The peaks are analysed by a curve fitting program assuming Gaussian lineshape. The peak at 2.15 eV corresponds to the first exciton transition and the peak at 3.04 eV corresponds to the second exciton transition. The experimentally observed transitions agree well with the theoretically calculated first and second exciton energies for PbS quantum dots using the four band envelope formalism [31]. This theoretical calculation is based on the nonparabolic and anisotropic band structure of this material and is the first theoretical calculation using an envelope function approach in the case of a narrow gap material.

### 3.3. Nonlinear absorption studies

From theoretical considerations, the resonant nonlinearity is expected to be enhanced in the regime of strong quantum confinement [6]. The ratio of the diameter of the nanocrystals to the Bohr radius is 0.19 in our system, indicating strong confinement and the resonant regime chosen for our studies gives rise to the large two-photon absorption coefficient.

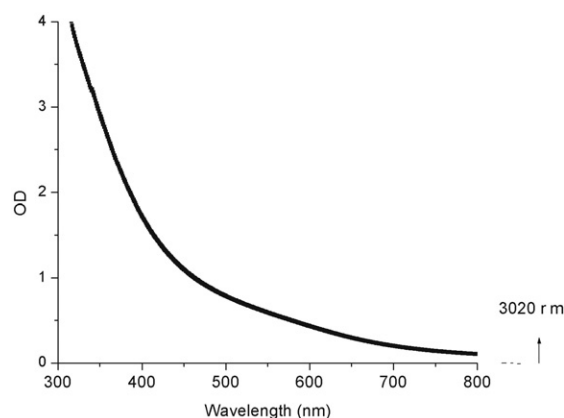


**Figure 5.** Optical absorption spectrum of PbS/glue nanocomposite P2.

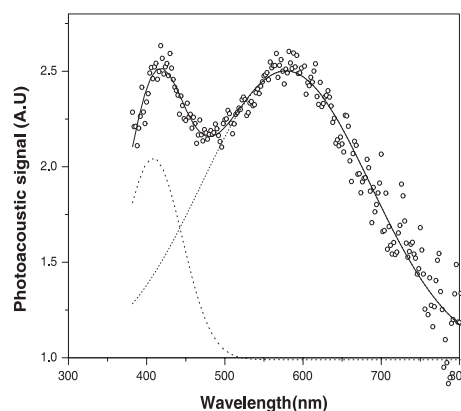


**Figure 6.** Photoacoustic spectrum of PbS/glue nanocomposite P2. The dashed line represents a Gaussian fit to experimental data.

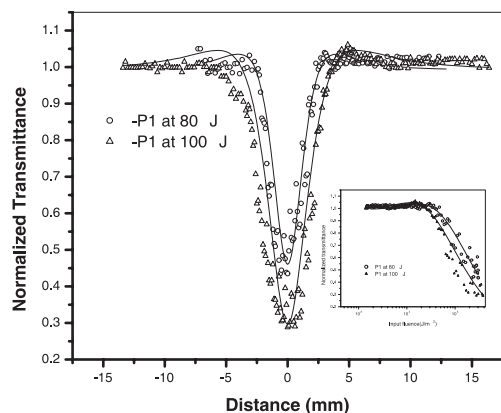
The PbSNC samples chosen for the nonlinear absorption studies are done on all four samples P0, P1, P2 and P4 (corresponding respectively to concentrations of 0.5, 1, 2 and 4 mM). For P0, the concentration was not sufficient to show nonlinearity. While the signal was clean at intermediate concentrations, obtaining a good signal-to-noise ratio was difficult at higher concentrations. The open aperture  $z$  scan is done at two excitation intensities,  $4.33 \times 10^9 \text{ W cm}^{-2}$  (laser pulse energy: 80  $\mu\text{J}$ ) and  $5.42 \times 10^9 \text{ W cm}^{-2}$  (laser pulse energy: 100  $\mu\text{J}$ ), respectively.

Figure 7 shows the open aperture  $z$  scans obtained for sample P1. The symbols denote experimental data points and the solid line is a theoretical fit incorporating saturable absorption followed by two-photon absorption (2PA). We consider a nonlinear absorption coefficient of the form [32]

$$\alpha(I) = \frac{\alpha_o}{1 + \frac{I}{I_s}} + \beta I \quad (1)$$

where  $\alpha_o$  is the linear absorption coefficient,  $\beta$  is the two-photon absorption (2PA) coefficient,  $I$  is the laser intensity and  $I_s$  is the saturation intensity. Therefore the modified normalized transmittance using equation (1) can be written as

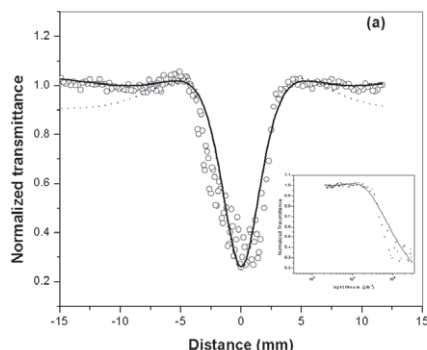
$$T(z) = \frac{Q(z)}{\sqrt{\pi}q(z)} \int_{-\infty}^{\infty} \ln[1 + q(z) \exp(-\tau^2)] d\tau \quad (2)$$



**Figure 7.** Z-scan curves of sample P1 at the excitation intensities  $4.33 \times 10^9 \text{ W cm}^{-2}$  (laser pulse energy:  $80 \mu\text{J}$ ) and  $5.42 \times 10^9 \text{ W cm}^{-2}$  (laser pulse energy:  $100 \mu\text{J}$ ). The experimental data are shown by symbols and the solid lines are numerical fits using a two-photon absorption model. The inset shows normalized transmittance of sample P1 at different intensities as a function of the input fluence.

where  $Q(z) = \exp(\alpha_o L I / (I + I_s))$ ,  $q(z) = \alpha_o I_o L_{\text{eff}} / 1 + (z/z_o)^2$  with  $I_o$  being the peak intensity at the focal point and  $L_{\text{eff}} = [1 - \exp(-\alpha_o L)] / \alpha_o$  where  $L$  is the sample length and  $z_o = \pi \omega_o^2 / \lambda$ , where  $\omega_o$  is the beam waist and  $\lambda$  is the light wavelength. The fitting is good and indicates that the mechanism here is saturable absorption followed by 2PA at higher intensities. The values of  $\beta$  and  $I$  are found to be  $2 \times 10^{-8} \text{ m W}^{-1}$  and  $3.2 \times 10^{12} \text{ W m}^{-2}$ , respectively, at  $4.33 \times 10^9 \text{ W cm}^{-2}$ . At  $5.42 \times 10^9 \text{ W cm}^{-2}$ ,  $\beta$  and  $I$  are  $3.2 \times 10^{-8} \text{ m W}^{-1}$  and  $1.95 \times 10^{12} \text{ W m}^{-2}$ , respectively. The 2PA coefficient is larger for the experiment with the larger intensity.

Figure 8(a) shows the open z-scan trace for sample P2 at the excitation intensity of  $4.33 \times 10^9 \text{ W cm}^{-2}$ . The symbols denote experimental data points. The data did not fit well into a theoretical fit corresponding to saturable absorption followed by 2PA (dotted line), and hence the analysis is modified incorporating saturable absorption and three-photon absorption (3PA) (solid line). The nonlinear absorption coefficient is now



taken as

$$\alpha(I) = \frac{\alpha_o}{1 + \frac{I}{I_s}} + \gamma I^2 \quad (3)$$

and the calculated normalized transmittance in this case is given by

$$T(z) = \frac{(1-R)^2}{\sqrt{\pi}} \frac{Q(z)}{p_o} \times \int_{-\infty}^{\infty} \ln \left[ \sqrt{1 + p_o^2 \exp(-2\tau^2)} + p_o \exp(-\tau^2) \right] d\tau \quad (4)$$

where  $p_o = [2\gamma(1-R)^2 I_o^2 L_{\text{2eff}}]^2$  with  $L_{\text{2eff}} = [1 - \exp(-2\alpha L)] / 2\alpha$ ,  $R$  is the surface reflectivity and  $\gamma$  is the 3PA coefficient. The best fit values obtained for  $\gamma$  and  $I_s$  are  $3.8 \times 10^{-18} \text{ m}^3 \text{ W}^{-2}$  and  $1.3 \times 10^{12} \text{ W m}^{-2}$ , respectively.

Figure 8(b) shows the z-scan trace of sample P2 at the higher intensity,  $5.42 \times 10^9 \text{ W cm}^{-2}$ . In this case, the best fit is obtained for three-photon absorption, taking the values of  $\gamma$  and  $I_s$  to be  $2.4 \times 10^{-18} \text{ m}^3 \text{ W}^{-2}$  and  $1.73 \times 10^{12} \text{ W m}^{-2}$ , respectively. The insets of figures 7 and 8 show plots of the normalized transmittance against input fluence for the respective samples.

Nonlinear optical response of semiconductor nanoclusters arises from a variety of physical mechanisms based on parameters such as the wavelength, pulse duration and intensity of the exciting radiation. Factors such as the nature of the surface of the nanocluster, the particle size and the distribution influence the response to a great extent. The processes involved in nonlinear absorption are generally free carrier absorption, multiphoton absorption, saturable absorption, etc.

Saturation absorption followed by optical limiting observed in the present case can be explained as follows. Due to the high surface-to-bulk ratio of these systems, the physical processes and mechanisms in these materials can be expected to depend strongly on the host matrix used. There is no chemical bond formation between the polymer molecules and the host matrix and the nanocrystals in the present case as mentioned earlier. There is only an interaction between the matrix and the nanocrystals, giving rise to the formation of trap states due to surface defects. Hence the observed saturable absorption is due to exciton bleaching in the presence of surface defects.

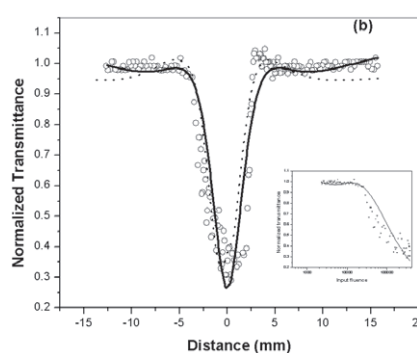


**Figure 8.** Z-scan curves of sample P2 at the excitation intensities (a)  $4.33 \times 10^9 \text{ W cm}^{-2}$  and (b)  $5.42 \times 10^9 \text{ W cm}^{-2}$ . Solid lines are numerical fits to the experimental data (shown by symbols) using three-photon absorption. Dotted lines are fits to two-photon absorption. Insets show the corresponding normalized transmittance of the sample as a function of input fluence. The solid line indicates fit to a three-photon absorption process.

The observed peak centred at 2.15 eV in photoacoustic spectroscopy corresponds to the first exciton transition energy as mentioned earlier. So the wavelength 532 nm (2.33 eV) used in the present experiment falls in the regime of 'above bandgap excitation' and overlaps with absorption due to transition energies beyond the first exciton transition. Patel *et al* [33] suggested a model for the electronic relaxation dynamics in PbS nanocrystals based on the results of transient absorption spectroscopy. When the nanocrystals are excited with a photon of energy above bandgap, the electrons are created as 'hot' carriers which nonradiatively relax quickly to the bottom of the conduction band and subsequently relax to the shallow trap states within the duration of a pulse less than 150 fs. The double exponential decay with time constants of 1.2 and 4.5 ps were obtained in their femtosecond measurements of photoexcited electrons. The authors have assigned the 1.2 ps decay of the trapped electrons from shallow trap states to deep trap states and the 4.5 ps component to electron-hole recombination from deep trap states. They have shown that the time constants are independent of pump power, probe wavelength, particle size, shape and surface capping. The laser pulses used for the present studies are of nanosecond duration which is greater than the lifetime of the states. Hence the nonlinear absorption observed here is mainly due to free carrier absorption (FCA). In addition, the values of  $\beta$  were found to be different at two different intensity levels for the sample P1 which also indicates that FCA is the predominant mechanism in our case. The observed nonlinear absorption in this case is mainly due to FCA arising from carriers photogenerated through 2PA.

Though the open  $z$ -scan plot in the case of sample P2 (figure 8) appears to fit well with a three-photon absorption model, the observed fifth-order ( $\chi^{(5)}$ ) nonlinearity might be an effective fifth-order (sequential  $\chi^{(3)}:\chi^{(1)}$  effect) nonlinearity arising from 2PA-generated carriers. Such a 2PA assisted excited state absorption has been previously reported for Au nanoparticles using 7 ns pulse duration excited at 532 nm even though a model based on the 3PA mechanism was fitted to the experimental data [34]. In an earlier paper, Banfi *et al* [35] have reported a fifth-order nonlinearity in semiconductor-doped glasses in the below-bandgap excitation regime arising from the refraction of photogenerated carriers through TPA. Due to the low repetition rate of the laser pulses (1 Hz), cumulative thermal effects are expected to be minimal in the present experiments. This is also indicated by the nature of the open  $z$ -scan trace.

#### 4. Conclusion

Stable nanocomposite films containing PbS nanocrystals of mean size 3.3 nm, in the regime of strong quantum confinement, are obtained by a simple and novel chemical procedure. The excitonic transition energies measured using photoacoustic spectroscopy are found to agree well with calculated values based on a four-band envelope formalism. The absence of bond formation between the semiconductor and the host materials leads to formation of surface defects which give rise to saturable absorption. The strong nonlinear absorption exhibited by the samples is probed by the open  $z$ -scan experiment. The large two-photon absorption coefficient

of the order of  $10^{-8} \text{ m W}^{-1}$  is attributed to strong quantum confinement in the resonant regime. The predominant mechanism of optical nonlinearity appears to be the absorption of free carriers generated by a 2PA process. The large nonlinear absorption gives rise to efficient optical limiting. These composite films also meet the requirements of transparency and high optical, thermal and chemical stability, apart from low cost, reproducibility and ease of preparation, and hence they are attractive candidate materials for nonlinear optical device applications.

#### Acknowledgments

Financial assistance from the Government of India is gratefully acknowledged. The authors PAK and CV also wish to acknowledge the Department of Science and Technology Unit on Nanoscience, IIT Madras for help in recording high resolution transmission electron micrographs.

#### References

- [1] Cotter D, Manning R J, Blow K J, Ellis A D, Kelly A E, Nessel D, Philips I D, Poustie A J and Rogers D C 1999 *Science* **286** 1523
- [2] Jiang H and Kakkar K K 1998 *Adv. Mater.* **10** 1093
- [3] Cartenuto G, Her Y S and Matijevic E 1996 *Ind. Eng. Chem. Res.* **35** 2929
- [4] Ekimov A I, Efros A I L and Onushchenko A A 1985 *Solid State Commun.* **56** 921
- [5] Brus L E 1984 *J. Chem. Phys.* **80** 4403
- [6] Schmitt-Rink S, Miller D A B and Chemla D S 1987 *Phys. Rev. B* **35** 8113
- [7] Eastoe J and Cox R A 1995 *Colloids Surf. A* **101** 63
- [8] Salata O V, Dobson P J, Hull P J and Hutchison J L 1994 *Adv. Mater.* **6** 772
- [9] Kuljanin J, Comor M I, Djokovic V and Nelejkovic J M 2006 *Mater. Chem. Phys.* **95** 67
- [10] Qiao Z, Xie Y, Chen M, Xu J, Zhu Y and Qian Y 2000 *Chem. Phys. Lett.* **321** 504
- [11] Zheng Z, Wang S and Yang S 1999 *Chem. Mater.* **11** 3365
- [12] Qiao Z, Xie Y, Zhu Y and Qian Y 1999 *J. Mater. Chem.* **9** 1001
- [13] Moller K, Bein T, Herron N, Mahler W and Wang Y 1989 *Inorg. Chem.* **28** 2914
- [14] Wang Y, Suna A and Mahler W 1987 *J. Phys. Chem.* **87** 7315
- [15] Borrelli N F and Smith D W 1994 *J. Non-Cryst. Solids.* **180** 25
- [16] Mukherjee M, Datta A and Chakravorty D 1997 *J. Mater. Res.* **12** 2507
- [17] Woggon U 1996 Optical properties of semiconductor quantum dots *Springer Tracts in Modern Physics* vol 136 (Springer)
- [18] Fick J and Martucci A 2004 *Encyclopedia Nanosci. Nanotechnol.* **4** 481
- [19] Lu S W, Soehling U, Mennig M and Schmidt H 2002 *Nanotechnology* **13** 669
- [20] Lin G and Xicheng A 2000 *Mater. Chem. Phys.* **63** 30
- [21] Ai X C, Guo L, Zou Y H, Li Q S and Zhou H S 1999 *Mater. Lett.* **38** 131
- [22] Martucci A, Fick J, Schell J, Bataglin G and Guglielmi M 1999 *J. Appl. Phys.* **86** 79
- [23] Martucci A, Innocenzi P, Fick J and Mackenzie J D 1999 *J. Non-Cryst. Solids* **244** 55
- [24] Fick J, Martucci A, Guglielmi M and Schell J 2000 *Fibre Integr. Opt.* **19** 43
- [25] Fick J, Schell J, Levy R, Martucci A and Guglielmi M 1997 *Pure Appl. Opt.* **6** 527
- [26] Li H P, Liu B, Kam C H, Lam Y L, Que W X, Gan L M, Chew C H and Xu G Q 2000 *Opt. Mater.* **14** 321

- [27] Nikesh V V, Dharmadhikari A, Ono H, Nozaki S, Ravindra Kumar G and Mahamuni S 2004 *Appl. Phys. Lett.* **84** 4602
- [28] He J, Ji W and Mi J 2006 *Appl. Phys. Lett.* **88** 181114
- [29] Rosencwaig A and Gersho A 1977 *J. Appl. Phys.* **47** 64
- [30] Sheik-Behae M, Said A A, Wei T M, Hagan D J and Van Stryland E W 1990 *IEEE J. Quantum Electron.* **26** 760
- [31] Kang I and Wise F K 1997 *J. Opt. Soc. Am. B* **14** 1632
- [32] Gao Y, Zhang X, Li Y, Liu H, Wang Y, Chang Q, Jiao W and Song Y 2005 *Opt. Commun.* **251** 429
- [33] Patel A A, Wu F, Zhang J Z, Torres-Martinez C L, Mehra R K, Yang Y and Rishbud S H 2000 *J. Phys. Chem. B* **104** 11598
- [34] Thomas J, Anija M, Cyraic J, Pradeep T and Philip R 2005 *Chem. Phys. Lett.* **403** 308
- [35] Banfi G P, Degiorgio V and Tan H M 1995 *J. Opt. Soc. Am. B* **12** 621